Cooperative Structure-Directing Effect of Fluorine-Containing Organic Molecules and Fluoride Anions in the Synthesis of Zeolites

Mar Arranz,[†] Joaquín Pérez-Pariente,*[,†] Paul A. Wright,[‡] Alexandra M. Z. Slawin,[‡] Teresa Blasco,[§] Luis Gómez-Hortigüela,[†,||] and Furio Corà[||]

Instituto de Catálisis y Petroleoquímica, C/Marie Curie 2, 28049 Cantoblanco, Madrid, Spain, School of Chemistry, University of St. Andrews, Purdie Building, North Haugh, St. Andrews, Fife KY16 9ST, United Kingdom, Instituto de Tecnología Química, Universidad Politécnica de Valencia-Consejo Superior de Investigaciones Científicas, Avenida de los Naranjos s/n, 46022 Valencia, Spain, and Davy Faraday Research Laboratory, The Royal Institution of Great Britain, 21 Albemarle Street, London W1S 4BS, United Kingdom

Received May 9, 2005. Revised Manuscript Received June 24, 2005

Dibenzyldimethylammonium (DBDM) cations, singly fluorinated at the ortho, meta, and para positions of the aromatic ring, have been investigated as structure-directing agents (SDAs) for the synthesis of all-silica zeolites in fluoride media and compared with the nonfluorinated molecule. The nonfluorinated DBDM cation can direct the synthesis either to an all-silica zeolite beta or to an all-silica zeolite ZSM-50 with the EUO framework topology. Under the same conditions that DBDM gives zeolite beta, benzyl-orthofluorobenzyldimethylammonium (*o*-FDBDM) readily directs the crystallization of pure all-silica ZSM-50 [*Cmma*, $a = 13.726(3)$ Å, $b = 22.171(5)$ Å, $c = 20.254(4)$ Å]. Replacing *o*-FDBDM by the para fluoro derivative (*p*-FDBDM) results in a much slower crystallization of ZSM-50 whereas no crystalline product results if the meta fluoro derivative (*m*-FDBDM) is added. Single-crystal diffraction studies of selected ZSM-50 crystals prepared using DBDM and *o*-FDBDM determine the location of the template and of charge-balancing fluoride atoms bound to framework silicon atoms and included within $[4^15^46^2]$ cages in the framework. Furthermore, the *o*-FDBDM is found to order within the structure, with the fluorine-containing aromatic rings occupying channel, rather than cavity, locations. Computer simulations indicate how the position of fluorine in the SDA influences the template ordering.

Introduction

The "templating effect" of organic molecules in the hydrothermal synthesis of zeolites is based on the experimental observation that there is a close geometrical relationship between the internal pore space defined by the zeolite framework and the surface of the occluded organic molecule.[1−4] Chemical interaction between the inorganic framework and the occluded organic takes place through both Coulombic and dispersive, nonbonding interactions. The dispersive forces are thought to play the decisive role in matching of the organic species to the zeolite cavities. The inclusion of organic molecules stabilizes the zeolite frameworks under the conditions of hydrothermal synthesis so that the organic species required to direct the crystallization of zeolite materials are called structure-directing agents (SDAs).[5] The exact role of SDAs remains a matter of debate; water-soluble aluminosilicate species organize around SDAs, and these entities are thought to be able to act as building blocks for the nucleation and growth of a particular zeolite phase.[6] Understanding the interactions between the organic and the zeolite framework is, therefore, necessary to achieve tailored zeolite synthesis.

Nonbonding interactions between the SDA and the zeolite cavity are dominated by those between hydrogen atoms at the surface of the SDA and the oxygens of the internal cavity walls. For all of the diverse compounds that have been used for zeolite synthesis, the character of the SDA−zeolite interaction is chemically similar. In this work we investigate the effect on the hydrothermal zeolite synthesis of changing the SDA's chemical character (and, therefore, the SDA−framework interaction) by replacing a proton by a fluorine atom. The size of a fluorine atom is only slightly larger than that of a hydrogen atom (the C−H bond length is 1.091 Å; that of C−F is 1.317 Å), so that it is possible to replace hydrogen by fluorine atoms in organic molecules without greatly affecting their shape and size.[7] In contrast, chemical, electronic, and surface properties would be expected to be more strongly affected. In general, for example, fluorine-containing organic species are more hydrophobic than their all-hydrogen counterparts.[8,9] Practically, for synthetic pur-

* Corresponding author. E-mail: jperez@icp.csic.es.
† Instituto de Catálisis y Petroleoquímica.
‡ University of St. Andrews.
§ UPV-CSIC.
|| The Royal Institution of Great Britain.

(1) Gies, H.; Marler, B. *Zeolites* **1992**, *12*, 42.
(2) Daniels, R. H.; Kerr, G. T.; Rollmann, L. D. *J. Am. Chem. Soc.* **1978**, *100*, 3097.
(3) Franklin, K. R.; Lowe, B. M. *Stud. Surf. Sci. Catal.* **1989**, *49*, 179.
(4) Ravishankar, R.; Kirschhock, C. E. A.; Knops-Gerrits, P. P.; Feijen, E. J. P.; Grobet, P. J.; Vanoppen, P.; De Schryver, F. C.; Miehe, G.; Fuess, H.; Schoeman, B. J.; Jacobs, P. A.; Martens, J. A. *J. Phys. Chem. B* **1999**, *103*, 4960.
(5) Lobo, R. F.; Zones, S. I.; Davis, M. E. *J. Inclusion Phenom. Mol. Recognit. Chem.* **1995**, *21*, 47.
(6) Goretsky, A. V.; Beck, L. W.; Zones, S. I.; Davis, M. E. *Microporous Mesoporous Mater.* **1999**, *28*, 387.
(7) Chambers, R. D.; Olah, G. A. *Fluorine in organic chemistry*; John Wiley & Sons: New York, 1973.

10.1021/cm050971j CCC: $30.25
Published on Web 07/26/2005

poses, the C−F bond is stable under hydrothermal synthesis conditions, provided the pH and temperature are not too high. The use of fluorinated organic molecules as SDAs for the synthesis of molecular sieves has been overlooked until very recently. Zones et al. reported the use of complex SDAs for the crystallization of SSZ-55, SSZ-53, and SSZ-59 by using fluorinated as well as nonfluorinated templates.[10,11] We have reported preliminary results of the use of fluorinated SDAs in the synthesis of both aluminophosphates and zeolites.[12] Here we report the detailed results of using mono-fluoro derivatives of dibenzyldimethylammonium (DBDM) as SDAs in the synthesis of pure silica zeolites.

We have studied the role of this SDA in the hydrothermal synthesis of all-silica phases because the hydrophobic character of fluorine-containing derivatives may make them more suitable for the crystallization of hydrophobic all-silica zeolite polymorphs rather than the more hydrophilic aluminosilicate zeolites. Furthermore, contributions to the total energy of the system due to interactions with the negative charge associated with framework aluminum may be avoided in this way. The synthesis is performed in fluoride media because this reduces the concentration of connectivity defects in zeolite materials.[13] A fully connected silicate framework is rendered negatively charged and, therefore, charge-balances the organic cation by the inclusion of fluoride ions that coordinate to silicon. DBDM has been selected as the SDA because of the ease of preparation of its fluoro-derivatives and also its known ability to direct the synthesis of several high silica zeolite phases of low framework density, the final product selectivity being strongly dependent upon the synthesis conditions. For example, zeolite beta,[14] which has a three-dimensional channel system with 12MR window apertures, zeolite ZSM-50,[15] with a pore system consisting of one-dimensional channels with a 10MR aperture and "side pockets", and zeolite ZSM-12,[16] with a one-dimensional channel system with a 12MR aperture, have all been synthesized in its presence. It should be noted that ZSM-50 has essentially the same silicate framework type as EU-1, prepared earlier by Casci et al. using the hexamethonium ion as SDA,[17] the structure of which was solved by Briscoe et al.[18] The framework topology code for these materials is EUO.[19] The different charge distribution of the templates is thought to influence the aluminum cation siting in ZSM-50 and EU-1,[20,21] so in an attempt to be consistent with the literature, we describe our DBDM-templated pure silica materials as pure silica ZSM-50.

Table 1. Chemical Analysis of C, H, and N[a]

	chemical analysis[b] (wt %)		
SDA	C	H	N
DBDMCl	71.98	8.76	5.35
	73.40	**7.70**	**5.35**
o-FDBDM	68.62	7.25	4.99
	68.69	**6.84**	**5.00**
m-FDBDM	68.28	7.30	4.99
	68.69	**6.84**	**5.00**
p-FDBDM	68.03	7.80	4.98
	68.69	**6.84**	**5.00**

[a] All samples contain some water. [b] Theoretical values in bold.

Experimental Section

The synthesis of dibenzyldimethylammonium chloride and its fluorinated derivatives was carried out by adding dimethylbenzylamine (Aldrich, +99%) drop by drop to a solution of benzyl chloride (99%, Aldrich) or *ortho*-fluoro-, *meta*-fluoro-, or *para*-fluoro-benzyl chloride (Avocado, 97%) with 10% of molar excess in ethanol kept in an ice bath. After 24 h at room temperature, the solution is removed under vacuum at 333 K and the resulting dibenzyldimethylammonium chloride or benzylfluorobenzyldimethylammonium chloride is washed repeatedly with diethyl ether and filtered. DBDMCl or FDBDMCl (~90% yield) are recovered. The products have been characterized by chemical analysis (Table 1) and ^{13}C magic-angle-spinning (MAS) NMR (see the following). The chloride salt was converted into the corresponding hydroxide, DBDMOH or FDBDMOH, by ion-exchange with an Amberlyst IRN78 resin (exch. cap: 4 mequiv/g, Supelco). The solution of DBDMOH or FDBDMOH obtained is titrated with 1 N hydrochloric acid (Panreac) and phenolphthalein (Aldrich).

The synthesis gel was prepared by adding tetraethylorthosilicate (Merck) to a DBDMOH or FDBDMOH solution with continuous stirring. Once the ethanol has evaporated, hydrofluoric acid (Panreac, 48 wt %) is added drop by drop. The resulting thick gel was introduced into 15-mL Teflon-lined stainless steel autoclaves which were heated at 408 K under static conditions for selected periods of time. The solid product was filtered, washed, and dried overnight at 333 K. The chemical compositions of the different synthesis gels and the crystallinity of the product phases are given in Table 2.

Solid products were first characterized by X-ray diffraction (XRD) to determine the product phase. Initially a Seifert XRD 3000P diffractometer, using Cu Kα radiation and operating in Bragg−Bentano geometry, was used. However, for samples of ZSM-50 the patterns were strongly affected by the preferred orientation of their large prismatic crystals. To minimize these pattern effects the samples were grounded, loaded into silica glass capillaries (0.7-mm o.d.), and examined on a STOE STAD i/p diffractometer operating with monochromated Cu $K\alpha_1$ radiation in Debye−Scherrer geometry. The capillaries were spun rapidly during data collection, which was over 12 h from 5 to 80° 2Θ. These diffraction patterns show an amorphous component resulting from scattering from the glass capillaries. The relative size of this component compared to the crystalline peaks varies as the packing density of the samples varies. The crystallinity of the solids was estimated by measuring the area under the peaks at 21−24° 2Θ

(8) Milioto, S.; Crisantino, R.; De Lisi, R.; Inglese, A. *Langmuir* **1995**, *11*, 718.
(9) Haszeldine, R. N.; Sharpe, A. G. *Fluorine and its compounds*; Methuen: London, 1951.
(10) Elomari, S.; Zones, S. I. *Stud. Surf. Sci. Catal.* **2001**, *135*, 479.
(11) Burton, A.; Elomari, S. A.; Chen, C.-Y.; Medrud, R. C.; Chan, I. Y.; Zones, S. I.; Bull, L. M.; Kibby, C.; Harris, T. V.; Vittoratos, E. S. *Chem.−Eur. J.* **2003**, *9*, 5737.
(12) Pérez-Pariente, J.; Gómez-Hortigüela, L.; Arranz, M. *Chem. Mater.* **2004**, *16*, 3209.
(13) Camblor, M. A.; Villaescusa, L. A.; Díaz-Cabañas, M. *Top. Catal.* **1999**, *9*, 59.
(14) Rubin, M. K. E.U. Patent 159,846, 1985.
(15) Rubin, M. K. U.S. Patent 4,640,829, 1987.
(16) Rubin, M. K. U.S. Patent 4,636,373, 1987.
(17) Casci, J. L.; Lowe, B. M.; Whittam, T. V. U.S. Patent 4,537,754, 1985.
(18) Briscoe, N. A.; Johnson, D. W.; Shannon, M. D.; Kokotailo, G. T.; McCusker, L. B. *Zeolites* **1988**, *8*, 74.
(19) http://www.iza-structure.org/databases. Accessed April 2005.
(20) Souverijns, W.; Rombouts, L.; Martens, J. A.; Jacobs, P. A. *Microporous Mater.* **1995**, *4*, 123.
(21) Peral, I.; Jones, C. Y.; Varkey, S. P.; Lobo, R. F. *Microporous Mesoporous Mater.* **2004**, *71*, 125.

Table 2. Gel Compositions, Products of Hydrothermal Syntheses at 408 K, and in Parantheses, Crystallinity of the Products, Expressed as a Percentage of the Most Crystalline Materials Prepared in This Work[a]

	experimental conditions						crystallinity				
SDA	experiment	SDAOH	SDACl	HF	SiO_2	H_2O	7d	15d	30d	45d	63d
DBDM	1	0.54	0.26	0.54	1	4.60	B (98)	B (100)			
	2	0.54	0.00	0.54	1	7.93		B (34)	B (75)	B (62)	
	3	0.44	0.00	0.44	1	7.93		E (7)	E (11)		E (100)
FDBDM	O-2	0.54	0.00	0.54	1	7.93		E (59)		E (46)	E (71)
	M-2	0.46	0.08	0.46	1	7.93		A	A	A	
	P-2	0.54	0.00	0.54	1	7.80		E (6)	E (10)		E (8)

[a] B = beta zeolite; E = ZSM-50 (EUO type); A = amorphous material.

Table 3. Experimental Parameters of the Single-Crystal Refinements of ZSM-50 Crystallized with *o*-FDBDM and Fully Protonated DBDM Cations

	o-FDBDM−ZSM-50	DBDM−ZSM-50
chemical formula	$C_{16}H_{19}FN[Si_{28}O_{56}F]$	$C_{16}H_{20}N[Si_{28}O_{56}F]$
formula weight	1945.8	1927.85
crystal system	orthorhombic	orthorhombic
space group	*Cmma*	*Cmm*a
Z	4	4
a (Å)	13.726(3)	13.771(7)
b (Å)	22.171(5)	22.304(11)
c (Å)	20.254(4)	20.326(10)
V (Å^3)	6164(2)	6243(5)
diffractometer	Rigaku MM007, with confocal optics	Rigaku MM007, with confocal optics
temperature (K)	93	93
λ (Å)	0.710 73	0.710 73
total no. of reflections	19 204	16 067
independent observed reflections ($I > 2\sigma I$)	2255	2081
2Θ range	1.84−25.35	2.01−25.35
R1 ($I > 2\sigma I$)	0.083	0.098
R1 (all data)	0.109	0.137
largest diff. e density (e·Å^{-3})	2.36, −0.909	0.922, −0.635

for the zeolite beta and at 23−24.5° 2Θ for zeolite ZSM-50. In each case the signal was corrected for diffuse scattering and the packing density and related to the most crystalline sample prepared in this work.

In addition, the materials were characterized by thermogravimetric analysis (TGA; Perkin-Elmer TGA7 instrument, heating rate 20 °C/min, air flow 30 mL/min), chemical analysis (Perkin-Elmer 2400 CHN analyzer), scanning electron microscopy (SEM; JEOL JSM 6400 Philips XL30 operating at 20 kV), and MAS NMR (Bruker AV 400 spectrometer, using a BL7 probe for ^{29}Si and ^{13}C and a BL2.5 probe for ^{19}F). ^{29}Si spectra were acquired using pulses of 3.3 μs (to flip the magnetization $3\pi/8$ rad) and a recycle delay of 240 s. ^{13}C cross polarization (CP) spectra were recorded using $\pi/2$ rad pulses of 4.5 μs and a recycle delay of 3 s. For the acquisition of the ^{13}C and ^{29}Si spectra, the samples were spun at 5−5.5 kHz at the magic angle. For ^{19}F spectra, $\pi/2$ rad pulses of 4.5 μs recycled delays of 80 s and spinning rates of approximately 20 kHz were used.

Single-Crystal Crystallography. Crystals of as-prepared ZSM-50 were selected from experiments 3 (protonated DBDM template, 63 days of heating) and O-2 (*o*-FDMDB, 63 days). These were mounted on glass fibers and examined on a Rigaku MM007 diffractometer, using a Mo Kα high-brilliance rotating anode equipped with Molymax confocal optics and an Xstream LT system. Data were integrated using CrystalClear. Structures were solved using SHELXS and refined using SHELXL (Table 3).[22] The final list of atomic coordinates and selected bond lengths and angles for O-2 are given in Tables 4−6. Details of the refined structures are discussed in the following.

Table 4. Atomic Coordinates, Fractional Occupancies, and Equivalent Isotropic Displacement Parameters (Å^2 × 10^3) for *ortho*-Fluorodibenzyldimethylammonium ZSM-50

	x	*y*	*z*	frac	*U* (eq)
Si(1)	0.2113(1)	0.432 68(8)	0.313 43(8)	1	0.0211(5)
Si(2)	0.3135(1)	0.374 43(8)	0.435 91(80	1	0.0223(5)
Si(3)	0.3862(2)	0.25	0.3846(1)	1	0.0256(6)
Si(4)	0.3886(2)	0.25	0.2335(1)	1	0.0263(6)
Si(5)	0.3103(1)	0.374 35(8)	0.191 70(8)	1	0.0211(5)
Si(6)	0.2129(1)	0.432 62(8)	0.071 41(8)	1	0.0213(5)
Si(7)[a]	0	0.4673(1)	0.0687(2)	1	0.0402(8)
Si(8a)	0	0.547(1)	0.2006(8)	0.5	0.020(3)
Si(9a)	0	0.4728(8)	0.3269(5)	0.5	0.016(2)
Si(10)	0	0.5463(5)	0.4581(4)	0.5	0.023(2)
Si(8b)	0	0.550(1)	0.1813(9)	0.5	0.029(4)
Si(9b)	0	0.4705(9)	0.3044(6)	0.5	0.028(3)
Si(11)	0	0.5745(5)	0.4298(4)	0.5	0.022(2)
F(in)	0.443(1)	0.317(1)	0.279(1)	0.25	0.061(6)
O(1)	0.25	0.5	0.3060(5)	1	0.057(3)
O(2)	0.0946(3)	0.4312(20	0.3178(30	1	0.038(1)
O(3)	0.2409(5)	0.3941(3)	0.2513(3)	1	0.056(2)
O(4)	0.2544(5)	0.4021(3)	0.3770(3)	1	0.071(2)
O(5)	0.3393(50	0.3068(3)	0.4204(3)	1	0.064(2)
O(6)	0.5	0.25	0.3968(5)	1	0.063(4)
O(7)	0.3595(6)	0.25	0.3093(3)	1	0.064(3)
O(8)	0.3325(5)	0.3047(2)	0.1969(3)	1	0.047(2)
O(9)	0.2531(4)	0.3849(2)	0.1238(2)	1	0.038(1)
O(10)	0.4062(50	0.4134(3)	0.1921(3)	1	0.070(2)
O(11)	0.25	0.5	0.0892(3)	1	0.031(1)
O(12)	0.25	0.3757(4)	0.5	1	0.067(3)
O(13)	0.4074(4)	0.4128(3)	0.4491(3)	1	0.070(2)
O(14)	0.0957(3)	0.4287(2)	0.0732(3)	1	0.039(1)
O(15)	0.5	0.25	0.2153(6)	1	0.068(4)
O(16)	0.25	0.4132(3)	0.0000	1	0.034(2)
O(17)	0	0.5157(7)	0.0193(7)	0.5	0.049(4)
O(18)	0	0.5275(6)	0.1052(7)	0.5	0.035(3)
O(19)	0	0.4931(80	0.1511(9)	0.5	0.055(4)
O(20)	0	0.4914(8)	0.2300(8)	0.5	0.050(4)
O(21)	0	0.5261(8)	0.2755(9)	0.5	0.058(5)
O(22)	0	0.5297(7)	0.3522(7)	0.5	0.036(3)
O(23)	0	0.4887(7)	0.4733(7)	0.5	0.049(4)
O(24)	0	0.4986(8)	0.3997(8)	0.5	0.051(4)
N(1)	0	0.25	0.1878(6)	1	0.039(3)
C(1)	0	0.3042(8)	0.2440(9)	0.5	0.024(4)
C(2)	0.088(1)	0.2788(7)	0.1894(7)	0.5	0.034(3)
C(3)	0	0.301(1)	0.125(1)	0.5	0.034(5)
C(31)	0	0.2765(8)	0.3120(8)	0.5	0.022(4)
C(32)	0.088(1)	0.25	0.3433(7)	1	0.061(4)
C(33)	0.0885(9)	0.25	0.4068(6)	1	0.051(3)
C(34)	0	0.25	0.439(2)	1	0.17(2)
C(41)	0	0.25	0.063(1)	1	0.077(6)
C(42)	0.0874(9)	0.25	0.0297(6)	1	0.040(3)
C(43)	0.086(1)	0.2825(7)	−0.0290(8)	0.5	0.041(4)
F(42)	0.159(3)	0.25	0.056(2)	0.5	0.19(1)

[a] Si(7) is the average Si position of two locations for silicon atoms in the two B chain configurations, each 50% occupied. These two locations could not be refined independently.

(22) Sheldrick, G. M. *SHELXL97*; University of Gottingen: Gottingen, Germany, 1987.

Table 5. Selected Bond Lengths in *o*-FDBDM−ZSM-50[a]

bond	distance (Å)	bond	distance (Å)
Si(1)−O(1)	1.591(2)	Si(7)′−O(17)	1.82(2)
Si(1)−O(2)	1.604(5)	Si(7)′−O(18)	1.525(14)
Si(1)−O(3)	1.575(5)	Si(7)″−O(14) × 2	1.571(5)
Si(1)−O(4)	1.570(5)	Si(7)″−O(17)	1.465(17)
Si(2)−O(4)	1.568(5)	Si(7)″−O(19)	1.764(18)
Si(2)−O(5)	1.573(2)	Si(8A)−O(10) × 2	1.566(17)
Si(2)−O(12)	1.564(5)	Si(8A)−O(19)	1.56(3)
Si(2)−O(13)	1.568(5)	Si(8A)−O(21)	1.59(2)
Si(3)−O(5) × 2	1.588(6)	Si(9A)−O(2) × 2	1.604(11)
Si(3)−O(6)	1.581(3)	Si(9A)−O(21)	1.58(3)
Si(3)−O(7)	1.570(7)	Si(9A)−O(24)	1.581(19)
Si(4)−O(7)	1.586(7)	Si(8B)−O(10) × 2	1.532(18)
Si(4)−O(8) × 2	1.616(5)	Si(8B)−O(18)	1.62(3)
Si(4)−O(15)	1.573(4)	Si(8B)−O(20)	1.64(3)
Si(4)−F(4)	1.91(2)	Si(9B)−O(2) × 2	1.587(2)
Si(5)−O(3)	1.599(5)	Si(9B)−O(20)	1.58(2)
Si(5)−O(8)	1.577(5)	Si(9B)−O(22)	1.63(2)
Si(5)−O(9)	1.600(6)	Si(10)−O(13) × 2	1.571(8)
Si(5)−O(10)	1.577(6)	Si(10)−O(23)	1.592(18)
Si(6)−O(9)	1.597(2)	Si(10)−O(24)	1.587(19)
Si(6)−O(11)	1.619(2)	Si(11)−O(13) × 2	1.594(8)
Si(6)−O(14)	1.611(5)	Si(11)−O(22)	1.622(16)
Si(6)−O(16)	1.593(2)	Si(11)−O(23)	1.573(19)
Si(7)′−O(14) × 2	1.571(5)		

[a] For static disorder in the framework (see text) the bond distances of silicons to the appropriate oxygens are included. Si(7) is the average Si position of two locations for silicon atoms in the two B chain configurations, each 50% occupied. These two locations could not be refined independently, so for Si(7), bond lengths around the two possible configurations are given.

Results and Discussion

Phase Selectivity as a Function of DBDM Chemistry. The initial stage in the experimental strategy was to optimize the conditions for the fully hydrogenated DBDM to exhibit maximum structure-directing activity. The product phases present were identified predominantly from the X-ray patterns. We have previously observed that DBDM leads to the spontaneous crystallization of all-silica zeolite beta,[23] optimum conditions for the crystallization of beta requiring low temperature, high concentration of SDA, and low water content (Table 2, experiment 1). Dilution of the gel and reduction of the SDA concentration strongly decrease the crystallization rate (Table 2, experiment 2). SEM (Figure 1) shows the truncated tetragonal bipyramidal morphology characteristic of beta zeolite, whose presence is identified also from XRD (Figure 2). The crystals obtained from the more diluted gel, sample 2, are larger and more elongated than crystals of sample 1, obtained from the concentrated gel. Further reduction in the SDA concentration effectively inhibits crystallization of beta, and in its place a minor amount of ZSM-50 is formed (Figures 1 and 2). The selectivity of DBDM in producing one or the other of these zeolites is strongly influenced by the reaction conditions; presumably because the nonbonding interaction energies of DBDM in zeolites ZSM-50 and beta are similar (the reported calculated nonbonded energies are −584 kJ/mol and −530 kJ/mol, respectively).[24] The strongest structure-directing behavior of an organic is likely to occur under conditions of relatively slow nucleation and growth but where reasonable yields are obtained over time periods during which the organic molecules will resist degradation. The conditions of experiment 2 fulfill these requirements and were, therefore, chosen for the examination of the behavior of fluorinated derivatives of DBDM as potential SDAs (Table 2).

Table 6. Selected Bond Angles of the Silicate Framework of *o*-FDBDM−ZSM-50[a]

moiety	angle (deg)	moiety	angle (deg)
O(1)−Si(1)−O(2)	111.0(2)	O(14)−Si(6)−O(16)	109.0(2)
O(1)−Si(1)−O(3)	110.4(4)	O(14)−Si(7)′−O(14)	113.4(4)
O(1)−Si(1)−O(4)	110.9(4)	O(14)−Si(7)′−O(17) × 2	116.0(3)
O(2)−Si(1)−O(3)	106.8(3)	O(14)−Si(7)′−O(18) × 2	116.7(3)
O(2)−Si(1)−O(4)	108.8(3)	O(17)−Si(7)′−O(18)	107.1(7)
O(3)−Si(1)−O(4)	108.8(4)	O(14)−Si(7)″−O(14)	113.4(4)
O(4)−Si(2)−O(5)	109.7(4)	O(14)−Si(7)″−O(17) × 2	116.0(3)
O(4)−Si(2)−O(12)	109.7(3)	O(14)−Si(7)″−O(19) × 2	116.7(3)
O(4)−Si(2)−O(13)	110.0(4)	O(17)−Si(7)″−O(19)	114.1(8)
O(5)−Si(2)−O(12)	108.0(4)	O(10)−Si(8A)−O(10)	110.5(17)
O(5)−Si(2)−O(13)	111.5(4)	O(10)−Si(8A)−O(19) × 2	111.0(9)
O(12)−Si(2)−O(13)	107.8(3)	O(10)−Si(8A)−O(21) × 2	105.6(10)
O(5)−Si(3)−O(5)	104.8(5)	O(19)−Si(8A)−O(21)	112.9(18)
O(5)−Si(3)−O(6) × 2	109.3(3)	O(2)−Si(9A)−O(2)	108.1(11)
O(5)−Si(3)−O(7) × 2	110.4(3)	O(2)−Si(9A)−O(21) × 2	110.8(6)
O(6)−Si(3)−O(7)	112.4(5)	O(2)−Si(9A)−O(24) × 2	108.4(6)
O(7)−Si(4)−O(8) × 2	108.9(3)	O(21)−Si(9A)−O(24)	110.2(14)
O(7)−Si(4)−O(15)	118.1(5)	O(13)−Si(10)−Si(13)	108.0(9)
O(8)−Si(4)−O(8)	97.3(4)	O(13)−Si(10)−Si(23) × 2	112.5(5)
O(8)−Si(4)−O(15) × 2	110.8(4)	O(13)−Si(10)−Si(24) × 2	107.3(6)
O(7)−Si(4)−F(4)[b]	68.2(7)	O(23)−Si(10)−Si(24)	108.9(11)
O(8)−Si(4)−F(4)[b]	79.8(6)	O(10)−Si(8B)−O(10)	114(2)
O(15)−Si(4)−F(4)[b]	74.5(7)	O(10)−Si(8B)−O(18) × 2	107.4(8)
O(3)−Si(5)−O(8)	109.5(3)	O(10)−Si(8B)−O(20) × 2	109.4(8)
O(3)−Si(5)−O(9)	108.5(3)	O(18)−Si(8B)−O(20)	109(2)
O(3)−Si(5)−O(10)	110.1(4)	O(2)−Si(9B)−O(2)	109.8(13)
O(8)−Si(5)−O(9)	107.2(3)	O(2)−Si(9B)−O(20) × 2	108.9(6)
O(8)−Si(5)−O(10)	112.1(4)	O(2)−Si(9B)−O(22) × 2	109.9(6)
O(9)−Si(5)−O(10)	109.5(3)	O(20)−Si(9B)−O(22)	109.3(15)
O(9)−Si(6)−O(11)	110.7(3)	O(13)−Si(11)−O(13)	105.8(8)
O(9)−Si(6)−O(14)	107.2(3)	O(13)−Si(11)−O(22) × 2	111.8(5)
O(9)−Si(6)−O(16)	108.3(3)	O(13)−Si(11)−O(23) × 2	108.6(6)
O(11)−Si(6)−O(14)	111.0(2)	O(22)−Si(11)−O(23)	110.0(10)
O(11)−Si(6)−O(16)	110.5(3)		

[a] Si(7) is the average Si position of two locations for silicon atoms in the two B chain configurations, each 50% occupied: bond angles around the two possible configurations are given for Si(7). Si(7)′ and Si(7)″ refer to the two different configurations around Si(7). [b] Fluoride F(4) is present at 25% occupancy.

The three mono-fluorinated derivatives of DBDM (o, m, and p substituted) were used as additives in the same molar ratio as in experiment 2. The details of the gel compositions, together with the product phases at different times (as identified by XRD) are given in Table 2 (experiments o-2, m-2, p-2). The results are clear and reproducible: *o*-FDBDM gives highly crystalline ZSM-50 whereas *m*-FDBDM gives no crystalline phases under these conditions and *p*-FDBDM gives only traces of ZSM-50 (Figure 3). Under exactly the same conditions the nonfluorinated template gives zeolite beta. Clearly both the inclusion of fluorine and its position within the ring strongly affect the structure-directing selectivity and effectiveness of DBDM. The ZSM-50 crystals formed in the presence of DBDM and *o*-FDBDM (experiment 3) are shown by SEM (see Figure 1) to be large and elongated, with similar aspect ratios (ca. 5) and typical lengths of 200 μm. The well-defined shapes are in direct contrast to those observed from syntheses of ZSM-50 under alkaline conditions, which are usually cuboidal or spherulitic and much smaller.[25] The ZSM-50 crystals prepared in this work are, therefore, suitable for single-crystal study.

(23) Arranz, M.; García, R.; Pérez-Pariente, J. *Stud. Surf. Sci. Catal.* **2004**, *154*, 256.
(24) Stevens, A. P.; Gorman, A. M.; Freeman, C. M.; Cox, P. A. *J. Chem. Soc., Faraday Trans.* **1996**, *92* (12), 2065.

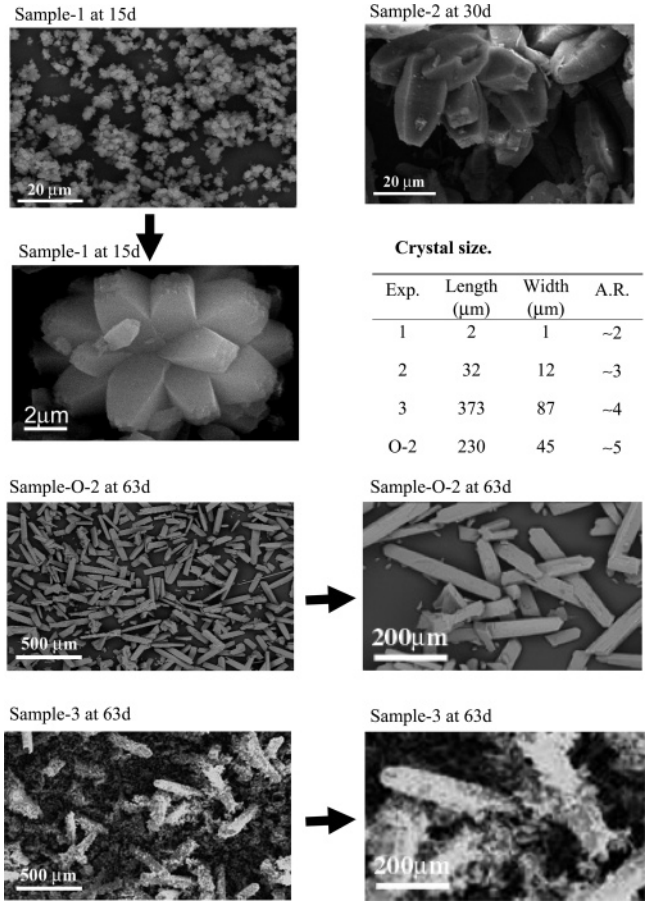

Figure 1. SEM of zeolite beta sample 1 and sample 2, ZSM-50 sample O-2, and ZSM-50 sample 3.

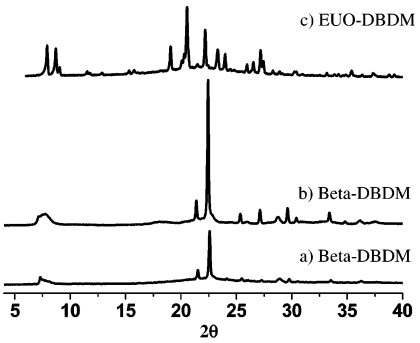

Figure 2. XRD patterns of phases obtained with DBDM as the SDA. (a) Sample 2 at 15 days (beta), (b) sample 1 at 15 days (beta), and (c) sample 3 at 63 days (ZSM-50).

Confirmation that the DBDM Species Are Included Intact: ^{13}C and ^{19}F MAS NMR. Comparison of the ^{13}C CP-MAS NMR spectra of the as-prepared zeolites and the solid ammonium salts shows that DBDM and *o*-FDBDM cations are present and intact within the as-prepared zeolites (Figure 4). The resonance signals of the CH_3 groups appear at 49 ppm, and those of the CH_2 groups appear at 73−78 ppm; for the *o*-FDBDM an additional signal is detected around 65 ppm, because the presence of the fluorine atom in the ring renders the methylene carbons nonequivalent. Aromatic carbons appear between 125 and 134 ppm and for the fluorinated cation there are two additional signals at 114 and 161 ppm, the last one from aromatic C−F.

^{19}F MAS NMR spectra of samples 2 (beta), 3 (ZSM-50), and O-2 (ZSM-50) are presented in Figure 5. The signal at

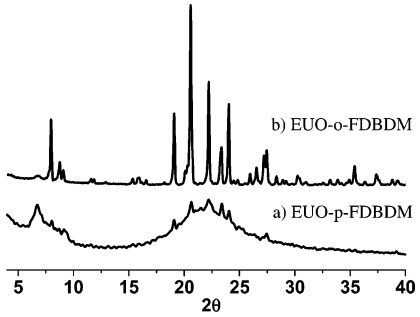

Figure 3. XRD patterns of phases obtained with fluorinated DBDM as the SDA at 63 days: (a) sample P-2, poorly crystalline ZSM-50, (b) sample O-2 (highly crystalline ZSM-50).

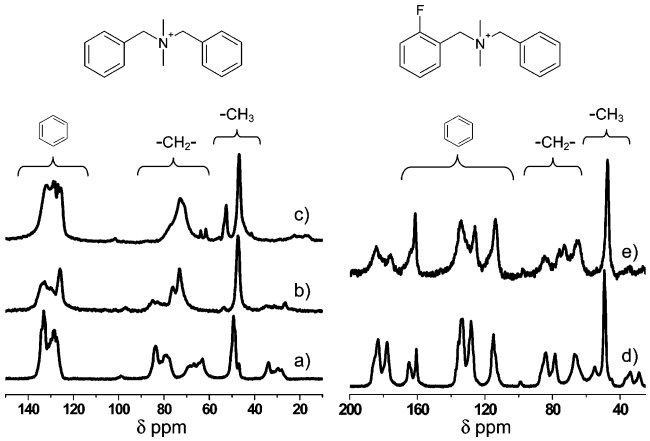

Figure 4. ^{13}C CP-MAS NMR of (a) DBDMCl salt, (b) DBDM beta sample 1 at 15 days, (c) DBDM−ZSM-50 sample 3 at 63 days, (d) *o*-FDBDMCl salt, and (e) *o*-FDBDM−ZSM-50 sample O-2 at 63 days.

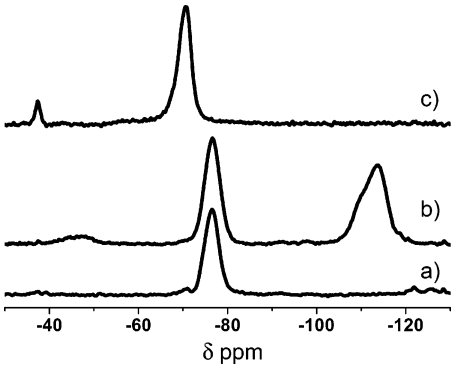

Figure 5. ^{19}F MAS NMR of (a) sample 3 at 63 days, DBDM−ZSM-50, (b) sample O-2 at 63 days, *o*-FDBDM-ZSM-50, and (c) sample 1 at 15 days, DBDM beta.

−114 ppm that can be observed in the spectra of the sample O-2 (ZSM-50) is due to the fluorine atom bonded to aromatic carbon in the ortho position,[26−28] which is additional evidence that indicates that *o*-FDBDM is occluded intact (Figure 5). The ^{19}F MAS NMR signal at low field corresponds to fluoride anions that compensate the positive charge of the SDA cations. The spectrum of the sample of beta-DBDMF from experiment 1 shows two signals at −70 and −37 ppm,

(25) Rao, G. N.; Joshi, P. N.; Kotasthane, A. N.; Ratnasany, P. *Zeolites* **1989**, *9*, 483.
(26) Simon, A.; Delmotte, L.; Chezeau, J. M.; Huve, L. *Chem. Commun.* **1997**, *3*, 263.
(27) Peralta-Cruz, J.; Meza-Toledo, S. E. *Magn. Reson. Chem.* **2004**, *42*, 81.
(28) Ariza-Castolo, A.; Guerrero-Alvarez, J. A.; Peralta-Cruz, J. *Magn. Reson. Chem.* **2003**, *41*, 49.

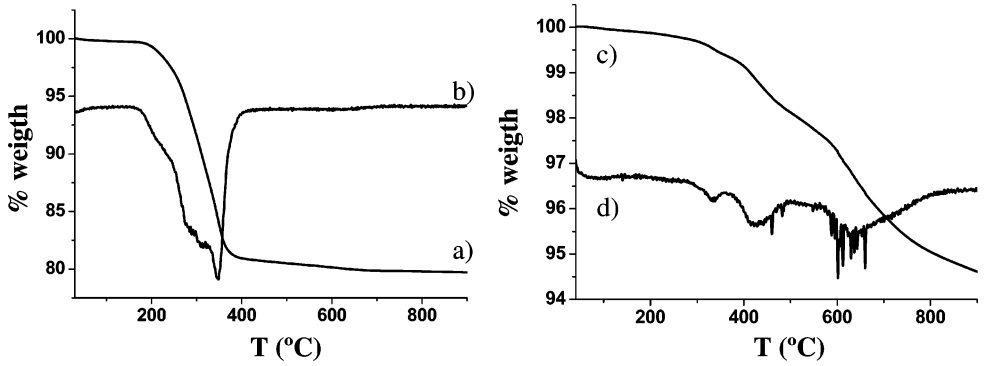

Figure 6. (a) TGA and (b) differential thermogravimetry (DTG) of zeolite beta sample 1, 15 days; (c) TGA and (d) DTG of zeolite ZSM-50, sample O-2, 15 days.

which are thought to be from fluoride anions present in cavities [$4^3 5^4$] and [4^6], respectively.[29] It is well-known that the topology of zeolite beta can be described as the intergrowth of two polymorphs, A and B, and even a third polymorph C. It is interesting to observe that the latter cavity is present only in polymorph C.[30] The cavity [$4^3 5^4$] is present in polymorph A or B, and from the spectrum of Figure 5 it can be estimated that 92% of the fluoride anions are present in this cavity. Both ZSM-50 materials show a signal at −76 ppm. This signal appears also in the clathrate nonasil,[29,31] where the fluoride is located in the [$4^1 5^4 6^2$] cage. The EUO framework topology is closely related to that of nonasil, and this [$4^1 5^4 6^2$] cage is present in both structures. Therefore, fluoride anions should be located in these cages.

Chemical Analysis and TGA To Estimate the Amount of DBDM in the Zeolite. Very little occluded water is found by TGA (Figure 6) in the as-made samples of beta and ZSM-50, as expected for hydrophobic pure silica zeolites. The zeolite beta sample shows about 20% weight loss between 300 and 400 °C, corresponding to removal of DBDM from the channels. Chemical analysis shows a C/N ratio of 16, suggesting that the DBDM cation is intact in the zeolite at a level of four molecules per unit cell. ZSM-50 samples show a small weight loss (∼5%) whereas chemical analysis shows an organic content of 12%. Even at 900 °C not all of the organic is removed, presumably due to blocking of some of the one-dimensional pores by structural defects. Nevertheless, DBDM and *o*-FDBDM are also shown by the chemical analysis to be intact (C/N 15.4 and 16.5, respectively) in the ZSM-50 samples, and there are, therefore, at least three DBDM cations per unit cell in both samples.

Structure Analysis of the ZSM-50 Samples. *Single-Crystal Diffraction.* The framework structure of EU-1 has been determined and refined previously from X-ray powder data and refined from neutron powder diffraction data for samples prepared under alkaline conditions.[18,21] The single crystals of the isostructural ZSM-50 obtained in this work are of sufficient quality to permit a full structure solution and refinement, giving details of cation location, fluoride ion siting, and framework geometry. Samples of ZSM-50 prepared with fluorinated and nonfluorinated DBDM were examined. The structural solution and refinement proceeded in a similar way for both materials.

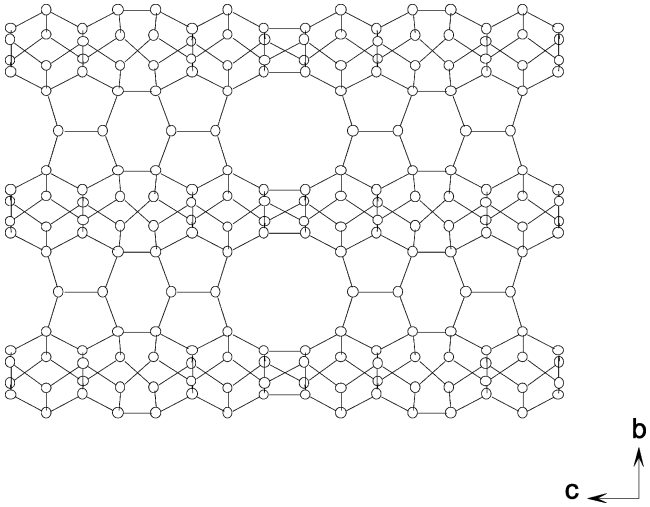

Figure 7. EUO framework topology, showing only the tetrahedral connectivity for clarity.

Structure solution was performed in the space group *Cmma*, as reported previously. This gave silicon and oxygen framework positions that were at first glance as expected for the EUO topology. However, there appeared to be disorder within the framework, and extra-framework scattering close to framework positions and within the pore spaces, so these were investigated further. The reported ZSM-50 structure consists of silicate layers linked by units comprising two [$4^1 5^4 6^2$] cages that share the four-membered ring. These double-cage pillaring units are arranged to give intersheet 10MR channels parallel to [100], with side pockets leading off the channel along [001] and [00$\bar{1}$], alternately. This is shown, for clarity without oxygens, in Figure 7. Within the layers, two different kinds of chains of silicate tetrahedra run parallel to the *c* axis and link within the plane of the layer, along [100]: a double chain of tetrahedra, A-type, and a single silicate chain, B-type (Figure 8). Close inspection of the single silicate B chains showed that there are two possible locations for each oxygen atom linking silicon atoms along the chain, and the silicon atoms Si(8), Si(9), and Si(10) refine with strongly anisotropic temperature factors, with residual electron density, either side of them. Furthermore, for these B-chain silicon atoms the Si−O

(29) Camblor, M. A.; Barrett, P. A.; Díaz-Cabañas, M.; Villaescusa, L. A.; Puche, M.; Boix, T.; Pérez, E.; Soller, H. *Microporous Mesoporous Mater.* **2001**, *48*, 11.
(30) Newsam, J. M.; Treacy, M. M. J.; Koetsier, W. T.; de Gruyter, C. B. *Proc. R. Soc. London, Ser. A* **1988**, *420*, 375.
(31) van de Goor, G.; Freyhardt, C. C.; Behrens P. *Z. Anorg. Allg. Chem.* **1995**, *621*, 311.

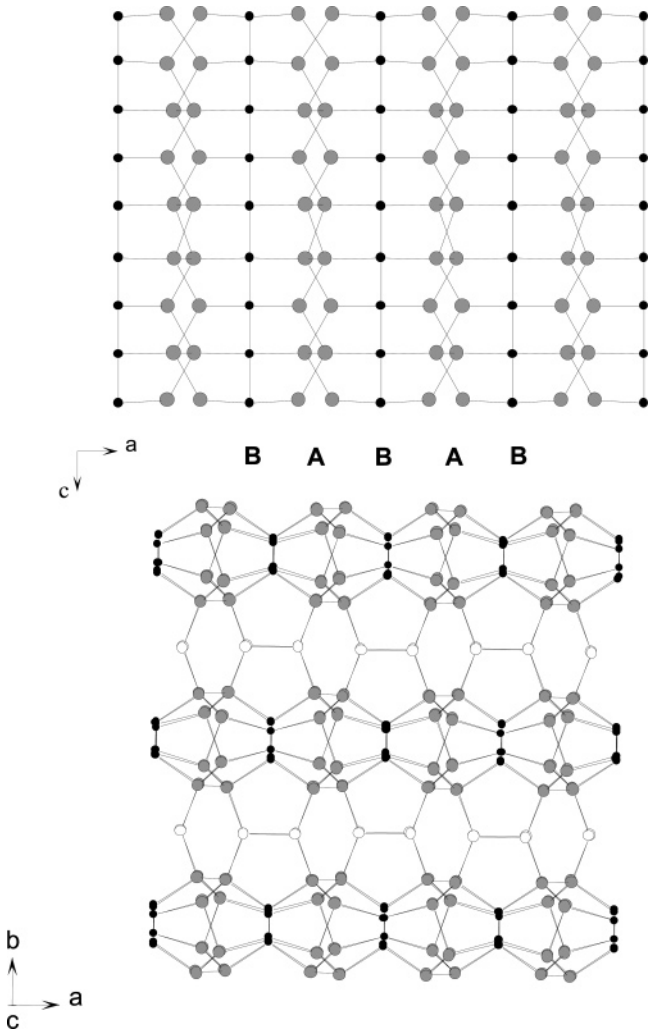

Figure 8. Two different kinds of chains of tetrahedra run parallel to the *c* axis in the silicate layers of structures with the EUO topology and link within the plane of the layer, along [100]: a double chain of tetrahedra, A type, and a single silicate chain, B type. These tetrahedral are represented as medium-grey and dark-gray spheres, respectively.

distances in the refinement differed widely from chemically reasonable values (1.4−1.9 Å). It was possible to split each Si(8)−Si(10) into two sites and to link each split silicon to two of the four oxygen positions along the direction of the chain. In this way two chain configurations, each with 50% occupancy, are observed and can be refined in a stable way, with much more reasonable bond lengths (Figure 9). The remaining silicon atom in the B chain was not as anisotropic as Si(8)−Si(10) and so was left as a single site, even though the Si(7)−O(18), O(19) bond distances [1.525(14) and 1.764-(18) Å] suggest this position is also an average of two sites, but they could not be refined independently. To check that this observation was not a result of too high a symmetry being chosen, structure solutions and refinements in alternative space groups *Cmm*2, *Cm*2*a*, and *C*2*mb* consistent with the observed reflections and absences were also attempted, but no improvement was observed in the fit. The same observation of two configurations for the B chain was made for the ZSM-50 prepared with nonfluorinated DBDM. It may, therefore, be concluded that the high resolution of the single-crystal diffraction experiment permits the resolution of two symmetry-related configurations of the B chain that occur, disordered, in different domains throughout the structure. Similar observation of two different configurations of a zeolite framework has recently been reported by Zones et al. for the pure silica polymorph of ZSM-23 (MTT).[32]

Difference Fourier analysis of the data also enables the fluoride anion that charge balances the organic cation to be located in the $[4^15^46^2]$ cages, as expected from the NMR (Figure 10). The occupancy of the site must be 0.25 to balance the template charge, which corresponds to one per "double cage" unit, disordered over the four sites. The exact location of the fluoride will change the local bond lengths and angles: by doing this it may consequently favor one of the two possible B chain conformations in the adjacent layer. No alternative space group symmetry that might result from ordering could be observed, suggesting that although there may be local ordering, these two features of the structure are averaged over the different sites over space and/or time.

The carbon and nitrogen positions of the DBDM SDA are also found directly within the structure, distributed over two symmetrically equivalent positions and occupying space in both sidepockets and channels (Figure 11). For atoms close to the mirror plane, it is difficult to resolve symmetry-equivalent positions, giving rise to a slight amount of apparent nonplanarity in the aromatic rings. Nevertheless the position of the SDA is found unambiguously and is very close to that predicted by energy minimization studies of Cox et al. for nonfluorinated DBDM.[33] Furthermore, and remarkably, the fluorinated ring is found to be located solely in the channel, rather than in the sidepocket. Attempts to detect fluorine at the ortho position of the other aromatic ring indicated that only hydrogen was present at this site. This specificity in the fluorine location may go some way to indicating how the fluorinated SDAs act differently than the nonfluorinated ones.

To confirm that the fluoride's position in the cages and the disorder in the framework chain are not a function of the SDA being fluorinated, the crystal structure of the sample from DBDM-containing gel was also examined. The same features of fluoride ion location, fluorine and framework disorder, and SDA location are observed, although in this case it is only possible to split Si(10) into two positions in the disordered chain, and as a result Si−O distances from Si(7), Si(8), and Si(9) are alternately too short (1.45−1.49 Å) or too long (1.79−1.89 Å). In fact, these silicon positions Si(7)−Si(9) are an average of the two true positions of the silicon atoms in each case.

X-ray Powder Diffraction Confirms that the Materials Are Phase Pure. Constrained Rietveld refinement of the ZSM-50 structure against the X-ray data was performed using the general structure analysis (GSAS) program[34] (Table 7). The refinements show that both samples consist of pure all-silica ZSM-50: the measured structures for the single-crystal data,

(32) Zones, S. I.; Darton, R. J.; Morris, R. E.; Huang, S. J. *J. Phys. Chem. B* **2005**, *109*, 652.
(33) Andrews, S. J.; Casci, J. L.; Cox, P. A.; Shannon, M. D. *12th International Zeolite Conference*, Baltimore, MD, July 5−10, 1998; Materials Research Society: Warrendale, PA, 1999; 2355.
(34) Larson, A. C.; Von Dreele, R. B. *General Structures Analysis System (GSAS)*; National Laboratory Report LAUR 86-748; Los Alamos National Laboratory: Los Alamos, 2000.

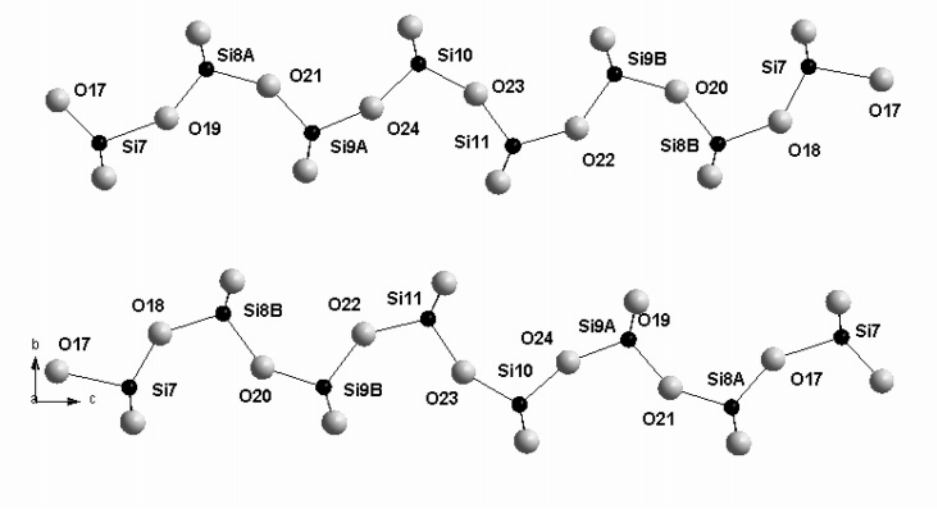

Figure 9. Two chain configurations of the single silicate B chains. Each has 50% occupancy.

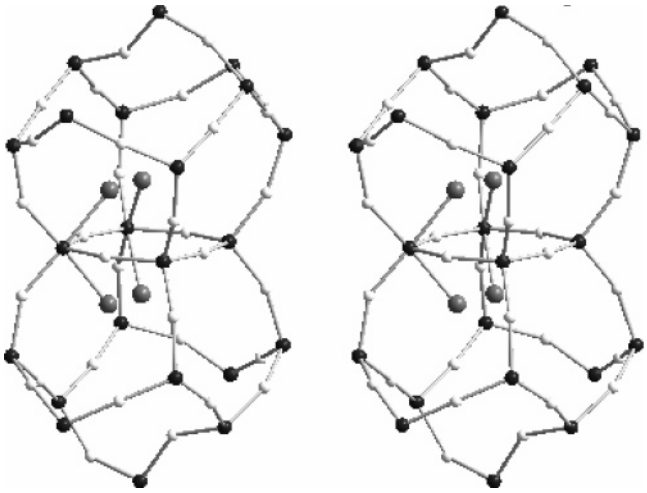

Figure 10. Difference Fourier analysis enables the fluoride anion that charge-balances the organic cation to be located in the [$4^1 5^4 6^2$] cages (represented here as a stereoview). Each fluoride position has 25% occupancy, and the positions of Si, F, and O are average positions. Grey, fluoride anions; white, oxygen atoms; black, silicon atoms.

Table 7. Crystallographic Data

	o-FDBDM−ZSM-50	DBDM−ZSM-50
pattern 2θ range	5−80	5−80
step scan increment (2θ)	0.02	0.02
space group	*Cmma*	*Cmma*
	Cell Constants	
a (Å)	13.7136(3)	13.7039(6)
b (Å)	22.2022(5)	22.2171(5)
c (Å)	20.2620(9)	20.2440(9)
R_{wp}	0.1189	0.0802
R_p	0.0920	0.0620
	Geometrical Restraints	
Si−O (Å)	1.60(0)	1.60(0)
O−O (Å)	2.6(0)	2.6(0)

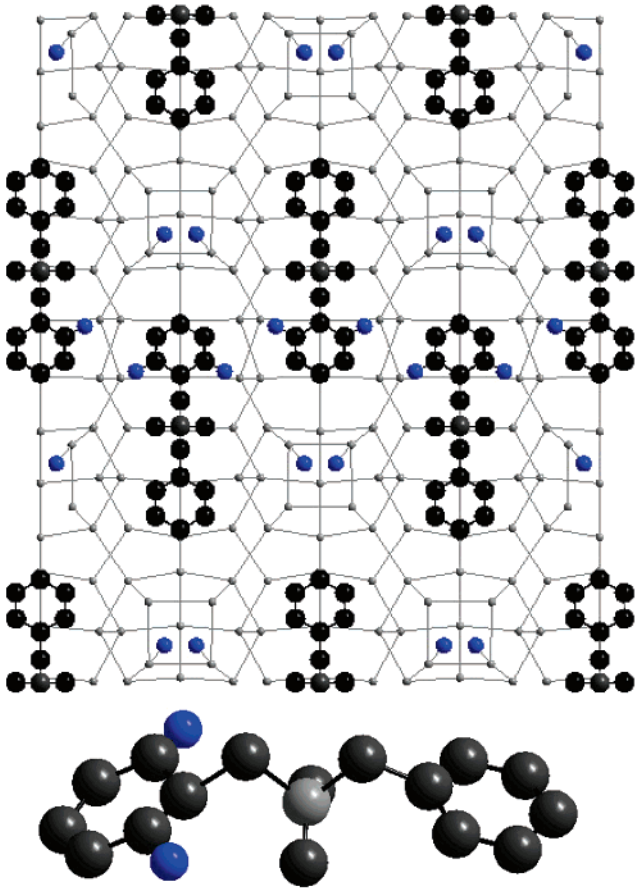

Figure 11. Crystallographically determined location of the SDA within the EUO framework (only the arrangement of tetrahedra is shown). The fluorinated ring is located solely in the channel, rather than in the side pocket, with each fluorine atom present at 50% occupancy (fluorine atoms and fluoride anions in blue, carbon in black, and nitrogen in dark gray).

including fluoride ion position, SDA location, and disordered chains fit the observed powder data closely. Lattice cell parameters of a = 13.7136(3) Å, b = 22.2022(5) Å, c = 20.2620(9) Å, R_{wp} = 11.89%, and R_p = 9.20% for *o*-FDBDMF−ZSM-50 (sample O-2 at 63d) and a = 13.7039(6) Å, b = 22.2171(5) Å, c = 20.2440(9) Å, R_{wp} = 8.0%, and R_p = 6.2% for DBDMF−ZSM-50 (sample 3 at 63d) are in agreement with the lattice cell parameters reported previously for the isostructural EU-1: a =13.695(1) Å, b = 22.326(1) Å, and c = 20.178(1) Å[18] (Figure 12).

Computational Study. To understand the difference in structure-directing ability between DBDM and its ortho-fluorinated derivative and the observed location of the ortho-fluorinated aromatic ring of the benzyl group in pure silica ZSM-50, a computational molecular-mechanics-based study was performed. Only the DBDM and *o*-FDBDM molecules

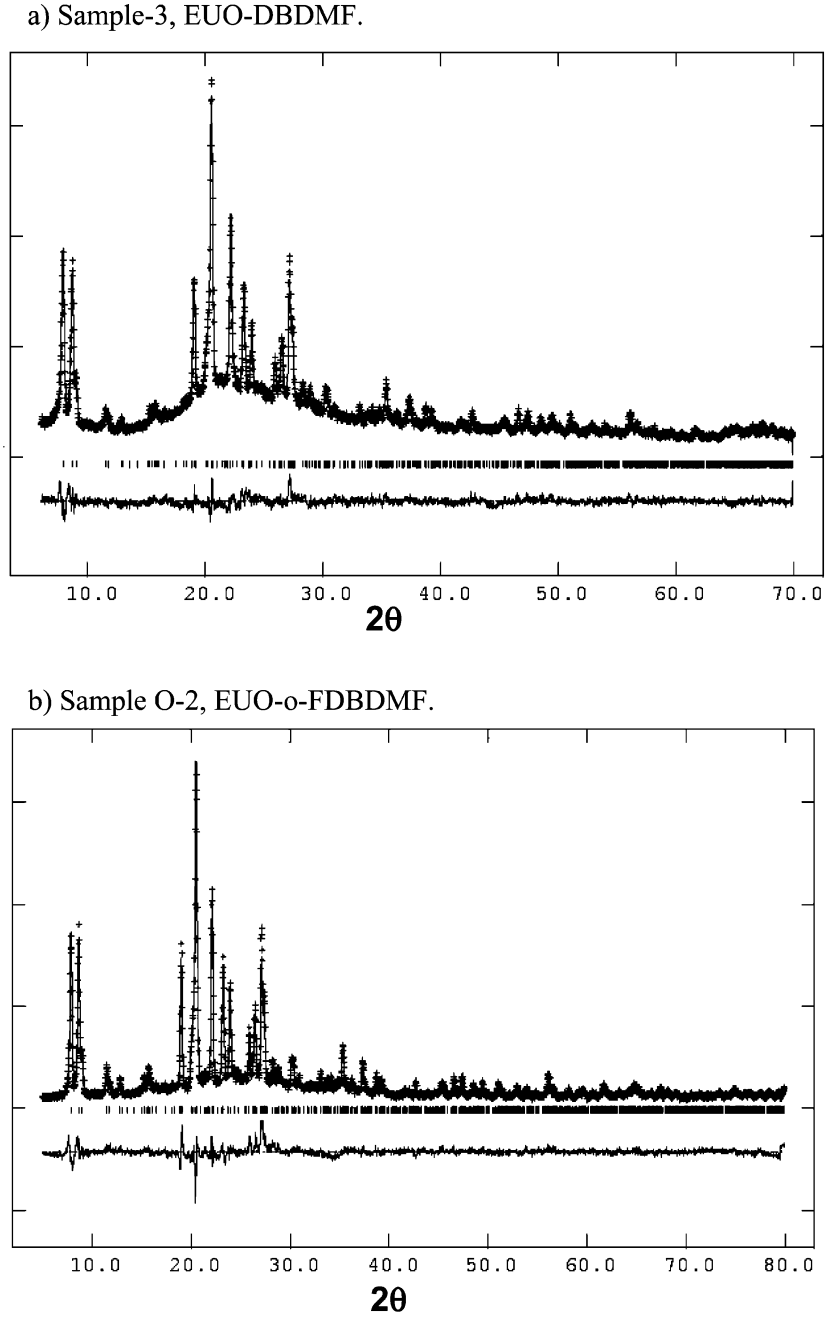

Figure 12. Observed, fitted, and difference X-ray powder diffraction profiles of constrained Rietveld refinements for as-prepared samples of, above, DBDM−ZSM-50 and, below, *o*-FDBDM−ZSM-50.

were studied, because the location of the fluoride anions is known from the crystal structure refinement only for these SDAs and not for the *p*-F and *m*-F derivatives.

The structure of the organic molecules and their interaction with the inorganic framework are described with the CVFF force field,[35] with van der Waals and Coulombic terms; the latter are calculated by Ewald summation. The zeolite structure[36] was kept fixed during all the calculations involving SDA molecules, taking the average position of Si atoms with half occupation. Periodic boundary conditions were applied to all the systems. The atomic charges inside the organic SDA cations were calculated by the charge-equilibration method,[37] under the constraint of a total net molecular charge of +1.

To determine which interactions are responsible for the ordered arrangement of the fluorinated phenyl groups of DBDM cations within the channel (rather than within the sidepockets), three types of interactions must be considered, separately or together: SDA···silica framework, SDA··· SDA, and SDA···fluoride ion. Modeling studies in which one or more of these interactions are excluded can highlight their relative importance.

(35) Dauger-Osguthorpe, P.; Roberts, V. A.; Osguthorpe, D. I.; Wolff, J.; Genest, M.; Hagler, A. T. *Proteins: Struct., Funct., Genet.* **1988**, *4*, 21.

(36) Briscoe, N. A.; Johnson, D. W.; Shannon, M. D.; Kokotailo, G. T.; McCusker, L. B. *Zeolites* **1988**, *8*, 74.

(37) Rappe, A. K.; Goddard, W. A., III. *J. Phys. Chem.* **1995**, *95*, 3358.

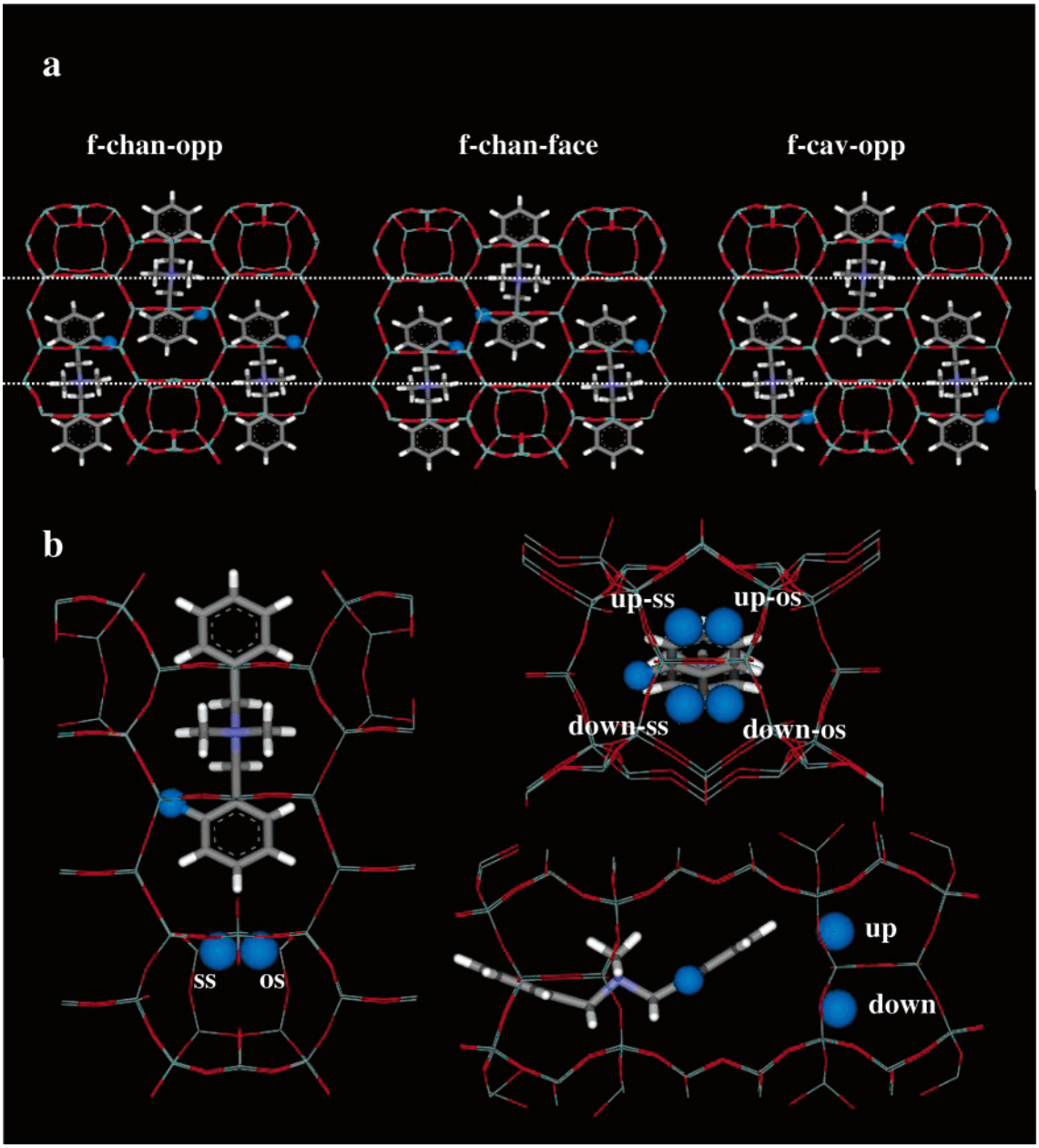

Figure 13. Relative orientation of *o*-FDBDM and fluoride anions in the simulations; (a) relative orientation of fluorinated SDA molecules (dashed white lines indicate the channel location); (b) relative orientation of fluoride anions with respect to the fluorinated SDA molecules.

Model 1: "No-Fluoride". We start first with a model in which no fluoride ion is present in the structure, which focuses on the interaction between the organic molecules and the zeolite structure. We label this model as no-fluoride. The net molecular charge of the SDA cations was compensated by the framework; charge-balance for the four $(SDA)^{1+}$ molecules in each unit cell was provided by decreasing uniformly the atomic charge of each silicon atom, from +2.4 (as in the CVFF force field for pure-silica zeolites) to +2.3643. The initial locations of the SDA molecules were the same as those obtained in the crystal structure refinement; four molecules were loaded in the unit cell. The final location of the molecules was obtained by geometry optimization of the systems, and the interaction energies were calculated by subtracting the energy of four isolated $(SDA)^{1+}$ cations optimized in a vacuum from the energy of the interacting system (framework + SDA molecules).

Two different locations are possible for the *ortho*-fluoro-SDA in the EUO structure type: the phenyl ring carrying the fluorine atom can be located in the cavity (f-cav configuration) or in the channel (f-chan). Furthermore, *o*-FDBDM molecules can be packed with fluorine atoms of adjacent molecules facing each other ("face" configuration) or on opposite sides ("opp" configuration; see Figure 13a), giving rise to four different configurations of the SDA molecules inside the framework. These four possibilities were studied for the ortho-fluorine derivative, and the resulting interaction energies are reported in Table 8 (no-fluoride model). The location of the molecules from the computational work was found to be essentially the same as measured in the experimental study.

The calculated energies show that packing of *o*-FDBDM molecules is much more stable when fluorine atoms locate on opposite sides (opp configuration), minimizing the F−F

Table 8. Calculated Interaction Energies, in kcal/mol per Unit Cell of Pure Silica EUO, for the Different Configurations and Models Described in the Text[a]

No-Fluoride Model

		o-FDBDM			
	DBDM	f-cav-opp SDA orientation	f-cav-face SDA orientation	f-chan-opp SDA orientation	f-chan-face SDA orientation
total interaction energy	−637.0	−638.5	−630.6	−642.6	−627.3

F$^-$−SDA Model

			o-FDBDM							
			f-cav-opp SDA orientation				f-chan-opp SDA orientation			
	DBDM		down F$^-$ orientation		up F$^-$ orientation		down F$^-$ orientation		up F$^-$ orientation	
	down F$^-$ orientation	up F$^-$ orientation	ss	os	ss	os	ss	os	ss	os
relat. Coul. energy	+31.7	**0.0**	+30.1	+43.4	**−0.8**	+20.9	+7.6	+14.6	**−29.1**	−19.3

[a] The zero point energy for the F$^-$−SDA model has been defined as the interaction energy of the DBDM-up configuration.

electrostatic repulsion. However, locating the fluorinated ring in the cavity or in the channel does not introduce a noticeable difference in the interaction energy of the *o*-FDBDM molecule with the framework. This suggests strongly that the ordering of fluorinated rings in DBDM within the channels rather than the cavities is not due to a destabilizing interaction with the framework atoms of theses cavities; in other words, there is enough space inside the cavity to host the fluorinated benzyl ring. The failure of this model to reproduce the experimental results seems to indicate that the main reason for the preferred location of the fluorinated benzyl ring in the channel must be associated with the presence of the fluoride anions, which are not accounted for in the no-fluoride model.

Model 2: Including the Coulombic Effect of Fluoride Ions "F$^-$−SDA". The next step was, therefore, to study the influence of the fluoride anions on the location and orientation of the fluorinated SDAs. The location of the fluoride anions is known from the crystal structure refinement, and that of the SDA molecules is known from both the experimental and the computational work described above. The shortest distance between fluoride and one of the SDA atoms is of ∼4 Å so that the van der Waals interaction between fluoride and SDA is negligible compared to their Coulombic interaction. We have, therefore, formulated a new simplified model to estimate the electrostatic interaction between fluoride and SDA ions, which we refer to as 'F$^-$−SDA'. In this model, the SDA molecules were positioned in the same location as that derived in the no-fluoride case (for each of the SDA orientations) and the fluoride anions inside the [$4^1 5^4 6^2$] cavities in the positions known from the experimental crystal refinement. Net atomic charges have been assigned to each atom of the SDA molecules according to the charge-equilibration method, and the formal charge of −1 has been assigned to the fluoride ions. We have then calculated the electrostatic energy associated with this distribution of charge. The framework atoms of the zeolite were removed from the calculation, to focus on the electrostatic interaction between SDA cations and fluoride anions in the required location for crystallization of ZSM-50. The periodicity of these models was the same as that for the zeolite structure, to include all the long-range ordered electrostatic terms in the crystal.

Four different locations of the fluoride anions within the [$4^1 5^4 6^2$] cavity are possible, known from the experimental results (see Figure 13b). These are symmetry equivalent with respect to the framework but not with respect to the SDA ions, and these four possibilities need to be evaluated individually. We refer to them as "up" and "down", "os" (other-side) and "ss" (same-side) relative to the orientation of the SDA molecule in the cage next to the fluoride position, as detailed in Figure 13b. All these configurations were built for DBDM and for the different orientations of *o*-FDBDM, and their electrostatic energies were calculated. The different interaction energies are shown in Table 8 (F$^-$-SDA model), taking as zero the energy for the DBDM-up case.

First of all, results clearly show that, in all orientations of the SDAs, the "up" position of the fluoride anions with respect to the organic cations is much more stable than the "down" one, probably due to a shorter distance of the fluoride ion from the benzyl ring in the neighboring channel. In the DBDM case, the two sides (os and ss) in which fluoride anions can locate are equivalent. However, the introduction of a fluorine substituent in the SDA breaks this degeneration. The most stable orientation occurs when fluorine from the SDA and fluoride anion are on the same side (ss). The most stable configurations for each possible orientation of the SDAs are shown in bold in Table 8. The *o*-FDBDM SDA with the fluorinated ring in the channel (f-chan) shows now a pronounced stability with respect to the nonfluorinated SDA and the fluorinated derivative in the f-cav configuration. This result is a clear indication that the higher stability of the ortho fluorine molecule when the benzyl ring containing the fluorine atom is located in the channel is due to a stabilizing electrostatic interaction with the fluoride ions. In the no-fluoride model, the energy range separating different orientations was of ∼15 kcal/mol; in the F$^-$−SDA model the energy range is of ∼30 kcal/mol (taking into account only the most stable fluoride position for each configuration of the SDAs in the structure, or up to 70 kcal/mol considering all the F$^-$ locations); this comparison strengthens the conclusion that it is the electrostatic interaction that is

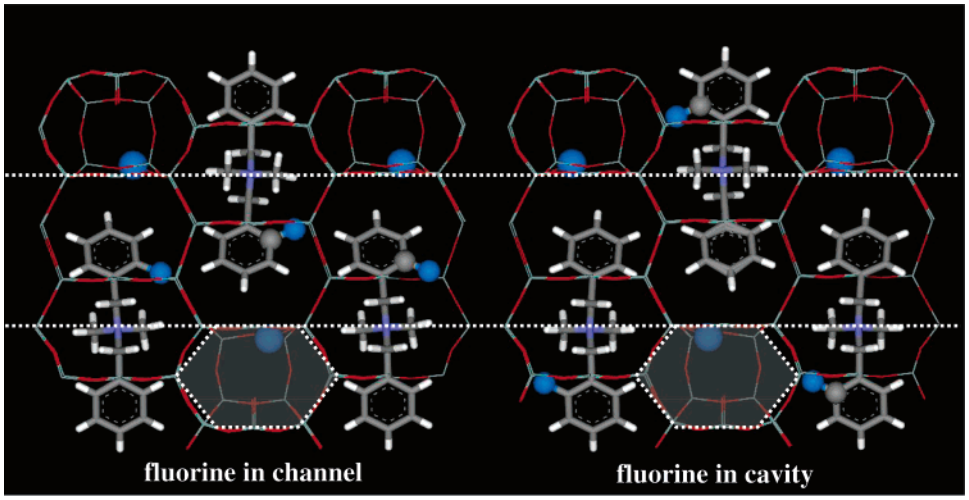

Figure 14. Relative orientation of *o*-FDBDM and fluoride anions in the EUO framework. Left: f-chan (see text) and fluoride in the most stable position (ss) in the "up" configuration. Right: f-cav (see text) and fluoride in the most stable position (ss) in the "up" configuration. F_C (blue) and C_F (grey) atoms of the C−F bonds and fluoride anions (blue) are displayed as balls (dashed white lines indicate the channel location).

responsible for the ordering of fluoride and SDA ions in the structure.

The introduction of fluorine in the SDA molecule induces the formation of a dipole between the carbon and the fluorine atoms of the new bond, with the carbon atom being positively charged and the fluorine atom negatively charged. The experimentally observed stabilization of the system due to the introduction of fluorine in the molecule involves the alignment of the C−F dipoles in the electrostatic field generated by the fluoride ions. The *o*-FDBDM SDAs orient in such a way as to approach the positively charged carbon atom (C_F) to the negative fluoride anion (F^-; stabilizing interaction) and move the negatively charged molecular fluorine (F_C) away from the fluoride anions (F^-; destabilizing interaction).

The relative locations of SDA and fluoride ions in the stable "up-ss" configurations are shown in Figure 14. The closest F_C-F^- distance (destabilizing interaction) is similar for both f-chan and f-cav configurations (5.98 and 5.92 Å in the up-ss configuration, respectively); however, the stabilizing interaction between the positive carbon atoms and fluoride anions is much more pronounced in the f-chan configuration (the closest C_F-F^- distance is 5.25 and 7.28 Å for f-chan and f-cav, respectively). The higher stabilizing interaction between the fluoride ion and the C−F dipole of the *o*-FDBDM molecule when the ring containing the fluorine atom is located in the channel prevents the molecules to orient in the f-cav configuration during the crystallization. Fluoride anions are thought to template the $[4^15^46^2]$ cavity structure (highlighted in gray in Figure 14), where they are in practice encapsulated at each stage of the framework growth. Once in this location, therefore, the fluoride ions would direct the orientation of the neighboring *o*-FDBDM molecules toward the "f-chan" configuration, in such a way as to maximize the stabilizing interaction between the positive part of the C_F-F_C dipole and the fluoride anion, hence, stabilizing the system, which is the main factor driving the self-assembly of fluoride and *o*-FDBDM ions toward the "f-chan-opp-up-ss" configuration observed experimentally.

Conclusions

It has been found that the role of DBDM cations as SDA for the synthesis of all-silica zeolites in fluoride media is strongly affected by the substitution of one hydrogen atom by a fluorine atom in one of the phenyl rings, and this effect has been observed to depend on the fluorine positioning in the ring. All-hydrogen DBDM leads to the spontaneous nucleation of zeolite beta, while the ortho-fluorinated cation allows the crystallization of ZSM-50 (framework type EUO), only traces of this phase are obtained for the para derivative, and no crystalline products are formed for the *m*-FDBDM cation. ^{13}C and ^{19}F MAS NMR show the cations to be intact inside the zeolite cavities, evidencing the stability of the C−F bond under the hydrothermal conditions present during the crystallization process. The electrostatic interaction between fluoride anions and the SDA molecules plays a determining role during the crystallization of the microporous material, determining the orientation of the SDA molecules inside the microporous structure.

Acknowledgment. Financial support of CICYT (Project No. MAT 2003-07769-C02-02) is acknowledged. M.A. and L.G.-H. also acknowledge the Spanish Ministries of Science and Technology for Ph.D. grants. We thank Accelrys for providing their software.

CM050971J